Geomechanics and Engineering, *Vol. 35, No. 2 (2023) 109-119*
https://doi.org/10.12989/gae.2023.35.2.109

Electrical resistivity survey and interpretation considering excavation effects for the detection of loose ground in urban area

Seo Young Song[1,4], Bitnarae Kim[1,5], Ahyun Cho[1], Juyeon Jeong[1], Dongkweon Lee[2] and Myung Jin Nam*[1,3]

[1]*Department of Energy and Mineral Resources, Sejong University, 05006 Seoul, Republic of Korea*
[2]*His Earth co. ltd., 04540 Seoul, Republic of Korea*
[3]*Department of Energy Resources and Geosystems Engineering, Sejong University, 05006 Seoul, Republic of Korea*
[4]*Korea Institute of Science and Technology, 02792 Seoul, Republic of Korea*
[5]*BRGM, Orléans, France*

(*Received April 7, 2023, Revised July 17, 2023, Accepted August 2, 2023*)

Abstract. Ground subsidence in urban areas due to excessive development and degraded underground facilities is a serious problem. Geophysical surveys have been conducted to estimate the distribution and scale of cavities and subsidence. In this study, electrical resistivity tomography (ERT) was performed near an area of road subsidence in an urban area. The subsidence arose due to groundwater leakage that carried soil into a neighboring excavation site. The ERT survey line was located between the main subsidence area and an excavation site. Because ERT data are affected by rapid topographic changes and surrounding structures, the influence of the excavation site on the data was analyzed through field-scale numerical modeling. The effect of an excavation should be considered when interpreting ERT data because it can lead to wrong anomalous results. A method for performing 2D inversion after correcting resistivity data for the effect of the excavation site was proposed. This method was initially tested using a field-scale numerical model that included the excavation site and subsurface anomaly, which was a loosened zone, and was then applied to field data. In addition, ERT data were interpreted using an existing in-house 3D algorithm, which considered the effect of excavation sites. The inversion results demonstrated that conductive anomalies in the loosened zone were greater compared to the inversion that did not consider the effects of excavation.

Keywords: electrical resistivity tomography; excavation; inversion; subsidence

1. Introduction

Subsurface cavities and subsidence occur not only in karst regions (Genis *et al.* 2018), but also in urban areas; causal factors include excessive development (Galvan *et al.* 2011, Hong *et al.* 2015, Kersten *et al.* 2017). Soil subsidence occurs frequently in downtown areas in South Korea, where soil is lost due to damage to aged underground sewer pipes (Kong *et al.* 2018). In addition, if the groundwater level (GL) becomes unstable during excavation conducted to construct new buildings, soil may flow into the excavation along with groundwater, resulting in ground subsidence (Ramirez *et al.* 2022). Ground subsidence in urban areas is a serious problem that can cause the collapse of surrounding facilities, such as buildings, and can cause loss of life.

Ground subsidence in urban areas has become a social issue in South Korea. Therefore, the Enforcement Decree of the Special Act on Underground Safety Management was enacted and came into effect in January 2022. In this decree, various ground safety assessment methods including geophysical surveys, such as ground-penetrating radar (GPR), electrical resistivity tomography (ERT), and seismic surveys, are required for projects involving tunneling and excavation work with a depth of ≥ 20 m (Liu *et al.* 2018, Lee *et al.* 2019, Prudhomme *et al.* 2019). Furthermore, after ground subsidence occurs, geophysical surveys can identify the extent of development of nearby underground cavities or weak zones, which is necessary before reinforcement work can proceed (Kim *et al.* 2007, Liu *et al.* 2023).

ERT provides subsurface electrical images at deep depths and has been widely used, but it can be affected by the surrounding environment in urban regions. It has been applied in various studies to identify fractured rock and cavities (e.g., Fountain *et al.* 1975, Smith 1986, Cardarelli *et al.* 2006, Kim *et al.* 2007, Ungureanu *et al.* 2017, Kidanu *et al.* 2020). Site characteristics affect the interpretation of resistivity data in urban areas experiencing subsidence. When analyzing the distribution of cavities and loose ground based on resistivity data, anomalies can occur; cavities have low resistivity in saturated conditions, and when there is a high water content (Galvan *et al.* 2011, Hong *et al.* 2015, Kidanu *et al.* 2020), while resistivity is high in unsaturated conditions (Ungureanu *et al.* 2017). In addition, when resistivity surveys are conducted near excavation sites, rapid changes in the current flow can have a large effect on resistivity data (Kim *et al.* 2022). A resistivity survey can be applied effectively in urban areas when the influence of the surrounding environment is considered.

*Corresponding author, Professor
E-mail: nmj1203@sejong.ac.kr

Copyright © 2023 Techno-Press, Ltd.

ISSN: 2005-307X (Print), 2092-6219 (Online)

ERT, despite being widely used in urban areas, encounters difficulties in data acquisition and interpretation due to the limited survey area, noise from surface or underground structures, and challenges with inversion resolution (Vickery and Hobbs 2002, Karaoulis *et al.* 2011, Chávez *et al.* 2014, Jang *et al.* 2018). The limitations of inversion resolution can lead to deviations from the actual resistivity values. To mitigate these issues, various methods have been employed, including data correction, utilization of diverse electrode arrays, and the application of constraints in the inversion algorithm. For instance, additional constraints such as smoothness, inequality, and active time constraints have been integrated into the inversion algorithm to enhance resolution and accurately calculate resistivity values (Samouëlian *et al.* 2005, Cardarelli *et al.* 2006, Sharma and Verma 2015, Jang *et al.* 2018). Moreover, Vickery and Hobbs (2002) addressed the effect of underground pipes by correcting the resistivity data.

In this study, ERT was performed in an urban area of South Korea where subsidence had occurred near an excavation site. To identify a loosened zone resulting from significant subsidence in an urban area, we utilized ERT. ERT has been established as a suitable geophysical method for urban environments, considering factors such as depth of investigation, urban noise, and spatial dimensions of the surveyed area (Soupios *et al.* 2008, Papadopoulos *et al.* 2018). The geological characteristics of the survey site and changes in the GL within the vicinity of the excavation area before and after subsidence occurred were analyzed. Before analyzing the data obtained by ERT in the vicinity of the excavation area, the effect of that area on the electrical response was analyzed using a field-scale 3D numerical model. For 2D inversion, we proposed to adjust the data according to the effect of the excavation area; this method proved effective when using a numerical model. The 2D inversion method considering the effect of excavation was applied to field data and used to interpret an area of loose ground. In the 3D inversion, the effect of the excavation site was considered through the application of an in-house inversion algorithm.

2. Site description

Subsidence has occurred during excavation work conducted at an urban construction site in Baekseok-dong, Ilsandong-gu, Goyang-si, Gyeonggi-do, South Korea (Fig. 1). After analyzing the geological structure of the site, we assessed changes in GL, which had been monitored even before subsidence occurred.

2.1 Geological structure

The study area is in Gyeonggi-do, where the major rocks are Jurassic granites, Precambrian banded gneiss of the Gyeonggi gneiss complex, and Quaternary alluvium (Yun *et al.* 2007). The banded gneiss of the Gyeonggi gneiss complex was formed by the metamorphism of sedimentary rock. The target area belonged to the Quaternary alluvium (Fig. 2(a)). Prior to the excavation, two boreholes (NX-1 and NX-2) were installed at the excavation site (Fig. 1(b)) to analyze the geological structure. The geological layers included a buried layer, sedimentary layer (sandy silt and gravelly sand), and soft rock (banded genesis) (Fig. 2(b)). The buried layer was 7.5 m below the surface and consisted of very loose granulated sand. The sedimentary layer could be further divided into an upper layer (about 7.5–22.5 m) mainly composed of silty sand and a lower layer (22.5–25 m) of dense silt and gravelly sand. The bedrock was characterized by cracks and joints. The GLs were 11.5 and 11.3 m from the surface at the NX-1 and NX-2 boreholes, respectively. The boreholes were at elevations of 0.7 and 0.1 m, respectively, and were about 20 m apart from each other.

2.2 Ground subsidence and fluctuations in GL during excavation

The 81 × 45.3-m excavation was made to a depth of 23.3 m and was longer in the northwest to southeast direction. During the excavation work, groundwater leakage carried soil into the excavation site on two occasions; this was considered to be the main reason for the subsidence. Subsidence occurred three times in 2017 on February 6, 14, and 22 (Fig. 1). The first and second subsidence events occurred after groundwater leakage into the excavation site from the southwest and northwest roads, respectively, while the third occurred after relatively minor cracking in the road caused by the first subsidence event. The center of the northwest road showed cracks of about 100 m during the second subsidence event, which was the largest of the three events. In the area of the second subsidence event, inclinometers (G1–6) were installed to measure surface settlement for 3 days (February 16−18). Settlements of up to 0.01 m were observed by G4–6, and a relatively large settlement occurred from the northeast to southwest direction (Fig. 3). The surface settlements in the G3 and G4, G5 and G6 from Feb. 16 to Feb. 18 corresponded respectively and overlapped in the Fig. 3.

Near the excavation site, six additional observation boreholes (W1−6) were installed to monitor GL with water gauges during construction, because fluctuations in the GL can serve as an indicator of the surrounding ground conditions. Boreholes W1 and W6 were located northeast of the excavation site, W2 and W3 were located to the southwest, and W4 and W5 were located to the northwest. The boreholes surrounded the excavation site and were numbered clockwise starting from W1 in the northeast. Boreholes W2 and W3 were located close to the area in which the first subsidence occurred, while W4 and W5 were located close to the area in which the second subsidence event occurred (Fig. 1).

The GL was measured at intervals of 1 week from September 12, 2016, but was measured 3–7 times a day after the first subsidence event (Fig. 4). Due to the excavation work, the GL at boreholes W1–W6 decreased by 0.84, 0.08, 0.2, 0.62, 0.58, and 0.8 m, respectively, compared to the GL before the excavation started (measured on January 25, 2017). When the first subsidence

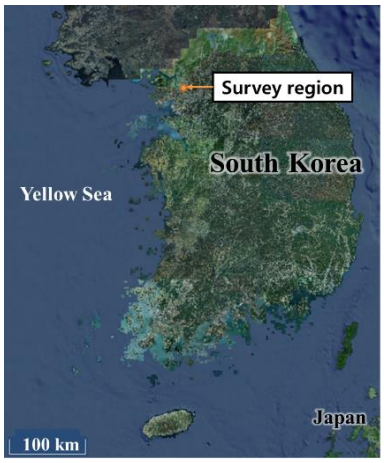

(a)

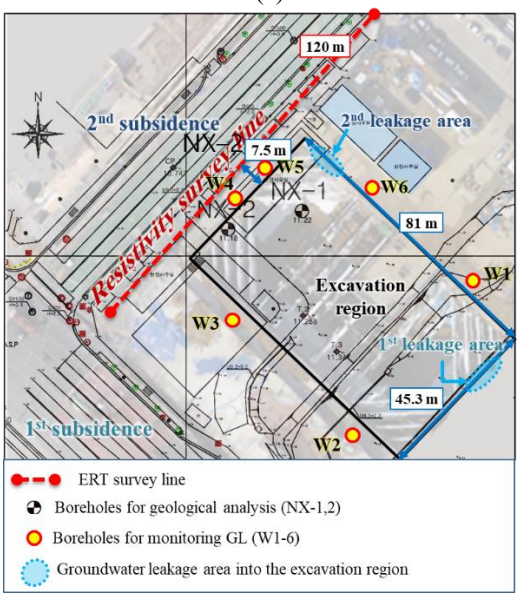

(b)

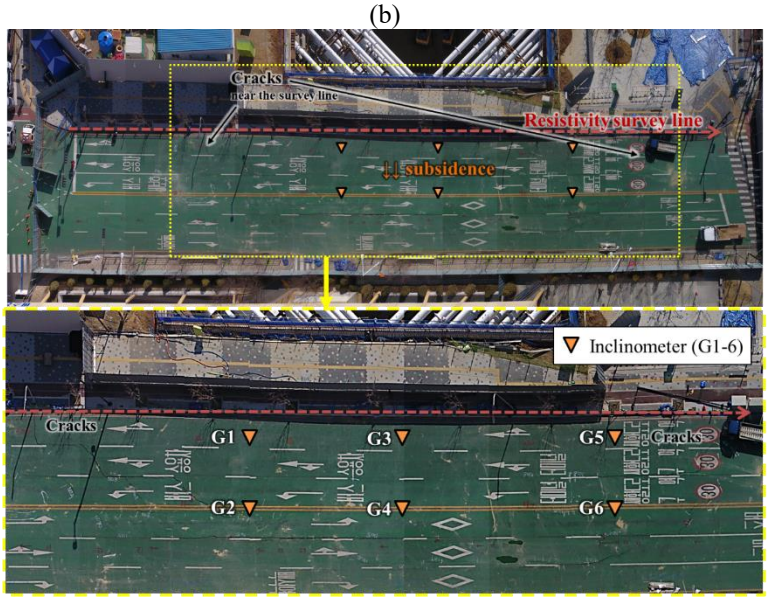

(c)

Fig. 1 (a) The survey region in the western part of Seoul, South Korea. (b) Schematic diagram showing the electrical resistivity tomography (ERT) profile (red dotted line) and boreholes used for the geological survey (NX-1 and -2) and groundwater level monitoring (W1−6). (c) Photograph of the area in which the second subsidence event occurred. The surface settlements were measured in the points of G1-6

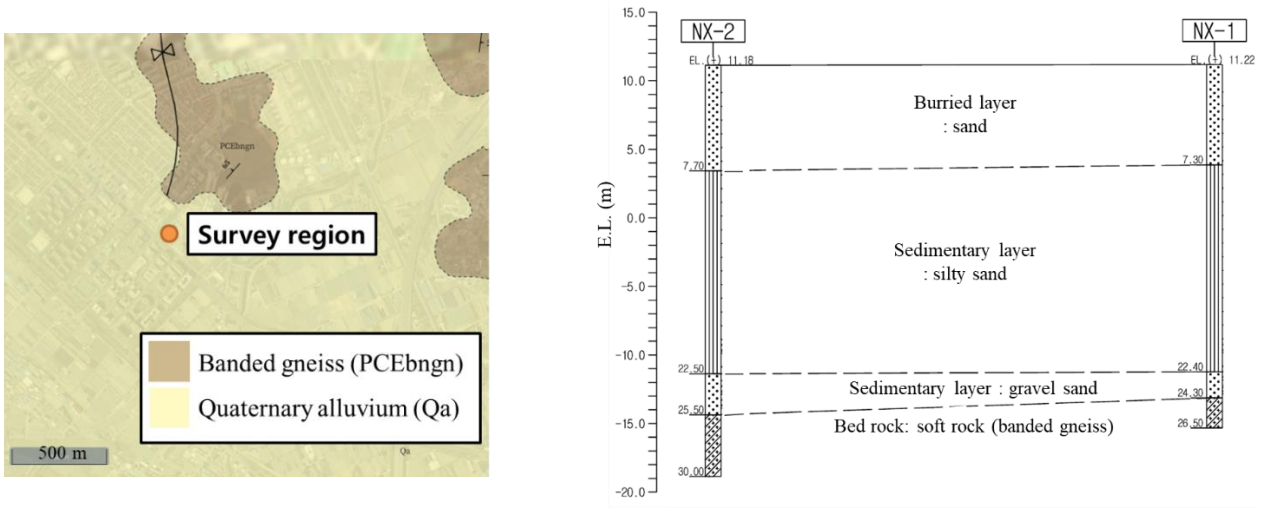

(a) (b)

Fig. 2 (a) Geological map of the survey region and (b) geological layers revealed by a drilling survey in boreholes NX-1 and NX-2

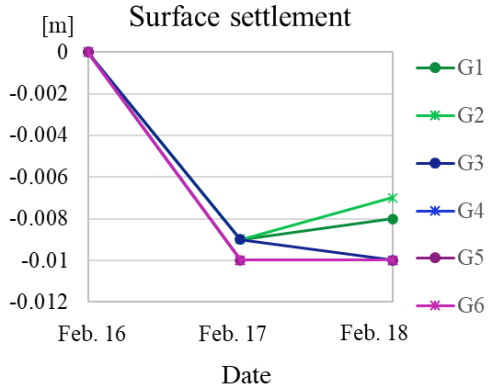

Fig. 3 Surface settlements measured by inclinometers G1−6 in the area in which the second subsidence event occurred

occurred on February 6, groundwater leaked rapidly and damaged the water gauge in borehole W2, which was located near the area in which the first subsidence event occurred. In borehole W1, the GL decreased by 1.06 m compared to that on February 5, and changed by 1.96 m cumulatively compared to the GL before the excavation work. In borehole W3, the GL decreased by 1.65 m over the same period (cumulative change of 1.87 m). After the sharp decrease in the GL in boreholes W1 and W3, the GL increased, but not to the same depth as before the subsidence. During the second subsidence event, the GL decreased by 5.54, 3.87, 2.14, 0.87, and 6.93 m for W1, W2, W4, W5, and W6, respectively, by February 14. These sharp deceases in the GL affected the subsidence.

3. The ERT survey at the urban site affected by construction-induced subsidence

The ERT survey was conducted on February 17, 3 days after the second subsidence event. To deploy a 120-m survey line, which was 7.5 m from the construction area and longer than the area of ground subsidence, bricks were removed from the sidewalk at intervals of 5 m to install stainless electrodes in the ground. Measurements were made with a dipole-dipole array having 10 n-spacing using an ABEM Terrameter LS (Guideline Geo, Stockholm, Sweden) (Fig. 5).

The measured voltage differences between the two receiving electrodes decreased with distance from the transmitter. Outliers, i.e., data that did not follow the decrease curve of the potential, were removed (Fig. 6). The average apparent resistivity near the surface was about 130 ohm-m and decreased as the n-spacing increased, with the lowest value being 11 ohm-m. Low resistivity can occur in layered earth due to the presence of a clay or fractured zone. Because the study site did not have a clay layer (Fig. 2), the low resistivity was considered to be due to subsidence.

4. Effects of the excavation site on ERT according to 2D inversion

Because the ERT line was near the excavation area, the ERT data could be affected by the excavation site, which contained highly resistive air. To analyze the effects of the air-filled excavation volume on the ERT data, we conducted numerical tests using a model constructed based on a region in Baekseok-dong where subsidence had occurred previously. After numerically simulating the ERT data for the model, 2D inversion of the data was performed to analyze the effects of the excavation site.

4.1 Numerical simulation of the effects of the excavation site on the ERT data

For the field survey of the target site, a field-scale 100 ohm-m half-space 3D numerical model was constructed that contained an excavation site (Fig. 7(a)) with non-conductive air (10^8 ohm-m). The excavation site had dimensions of 80

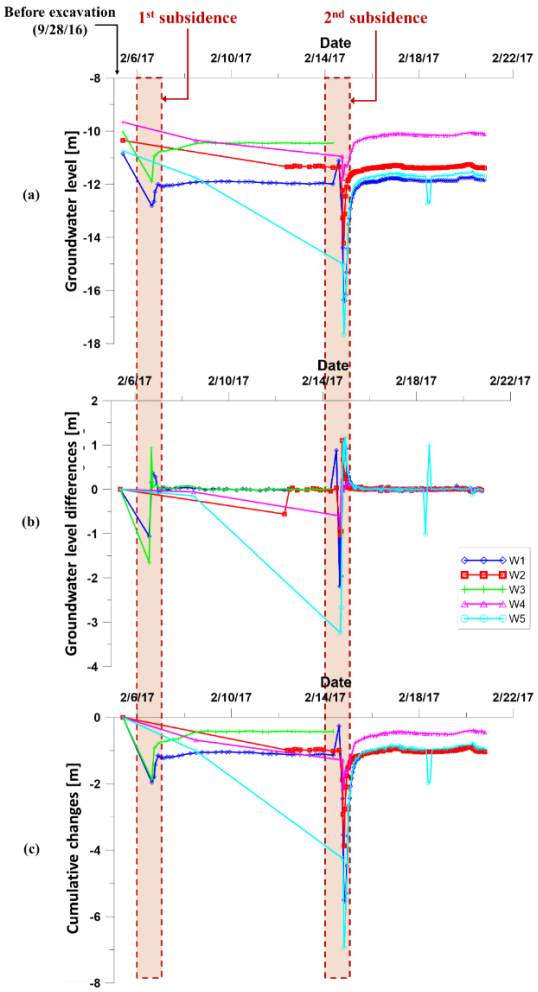

Fig. 4 (a) Groundwater level (GL) fluctuations recorded from September 28, 2016 to February 21, 2017, in monitoring wells W1−5. Changes in GL compared to a previous measurement (b) and to the first measurement before excavation (cumulative change) (c) were also shown

× 45 m in the x- and y-directions, respectively, with a depth of 20 m (z-axis). The ERT line was 120 m long in the y-direction and 7.5 m from the excavation area, with an electrode spacing of 5 m (10 n-spacing) that replicated the actual field survey. The ERT data resulting from the 3D modeling were compared with the data from a homogeneous 100 ohm-m background model that did not contain an excavation site. The apparent resistivity in the excavation site model was about 1.87 times (Fig. 7(c)) higher compared with the background model (Fig. 7(b)). The increase became larger with larger n-spacing due to the presence of the excavation site, indicating that ERT data obtained near an excavation site should be inverted to take account of the effects of excavation.

4.2 Correction of distorted ERT data for 2D inversion considering excavation effects

Because 2D inversion assumes no changes in the strike direction, distortion of the ERT data caused by the presence of an excavation site can be misinterpreted due to the 3D nature of the site. We therefore corrected distortion of the ERT data before performing 2D inversion to account for the effects of the excavation site. The correction was conducted by dividing the ith apparent resistivity (ρ_{ai}) near the excavation site, with the ratio (r_i) between the apparent resistivities near the excavation site (ρ_{ai}) and in a model without an excavation site (ρ_{bi}) being obtained as follows

$$r_i = \rho_{ai}/\rho_{bi}. \quad (1)$$

Using the above equation, the effect of distortion by the excavation site could be removed from the apparent resistivity data.

4.3 Correction of a 2D inversion of the ERT data for a 3D excavation site

The ERT data in the 2D survey line near the excavation site could be obtained through 3D modeling. The 3D modeling was conducted twice, using a half-space homogeneous model (100 ohm-m) including a conductive anomaly with and without an excavation region (Figs. 8(a) and 8b)). The conductive anomaly was assumed to be caused by loose ground 10 ohm-m below the survey line. It extended for 35 and 15 m in the x- and y-directions,

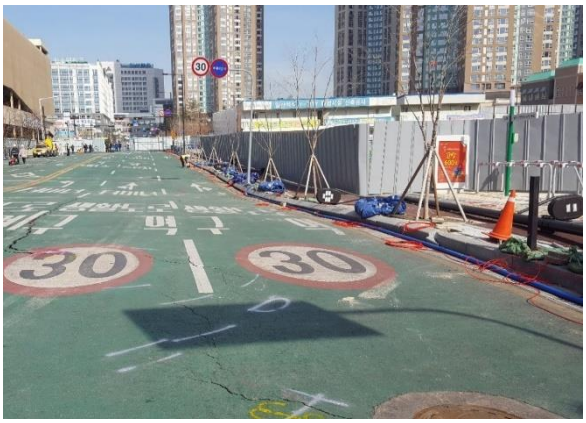

(a)

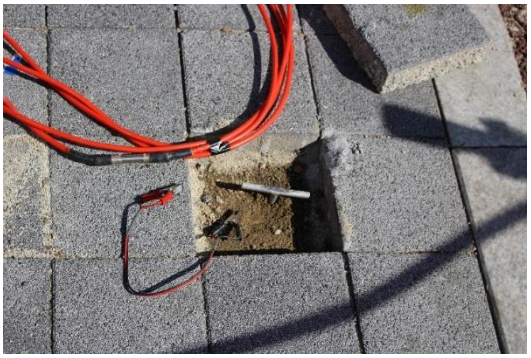

(b)

(c)

Fig. 5 (a) Electrical resistivity tomography (ERT) profile between the excavation site and a road in the urban area. (b) Stainless electrodes were installed in the sidewalk after removing paving blocks. (c) The 64-channel ABEM Terrameter LS instrument used for the ERT survey

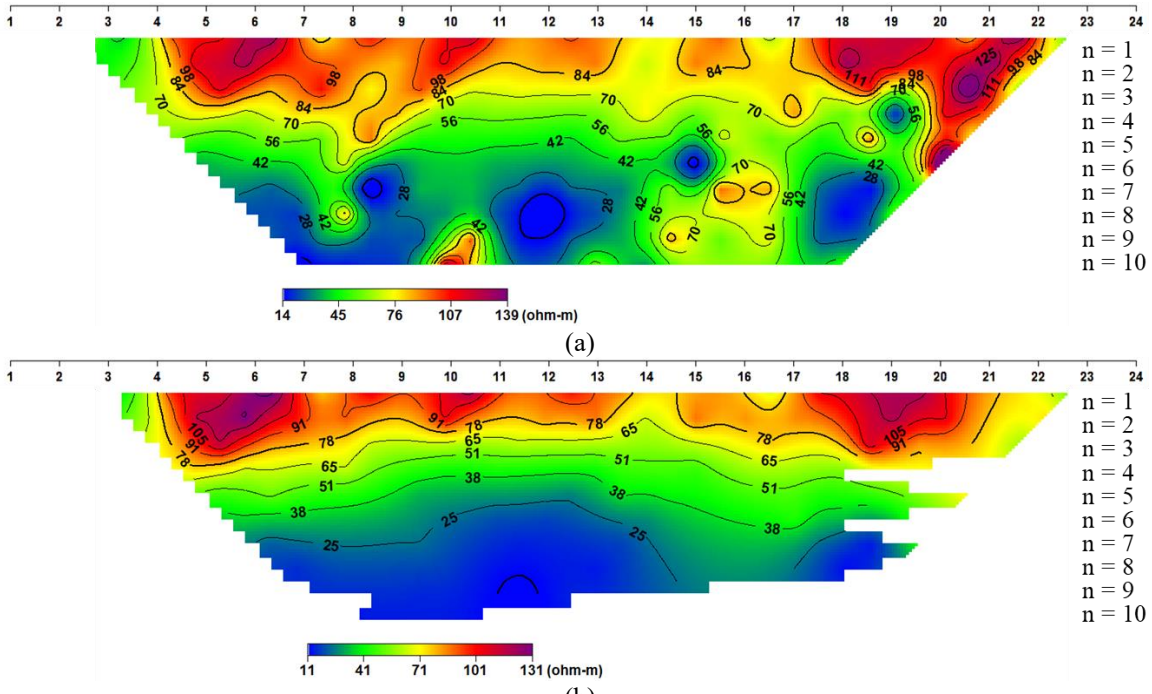

(a)

(b)

Fig. 6 Apparent resistivity data obtained by electrical resistivity tomography (ERT) performed near the excavation site. (a) Raw data and (b) data obtained after deleting outliers, i.e., data that did not follow the curve of the potential for each transmitting electrode pair

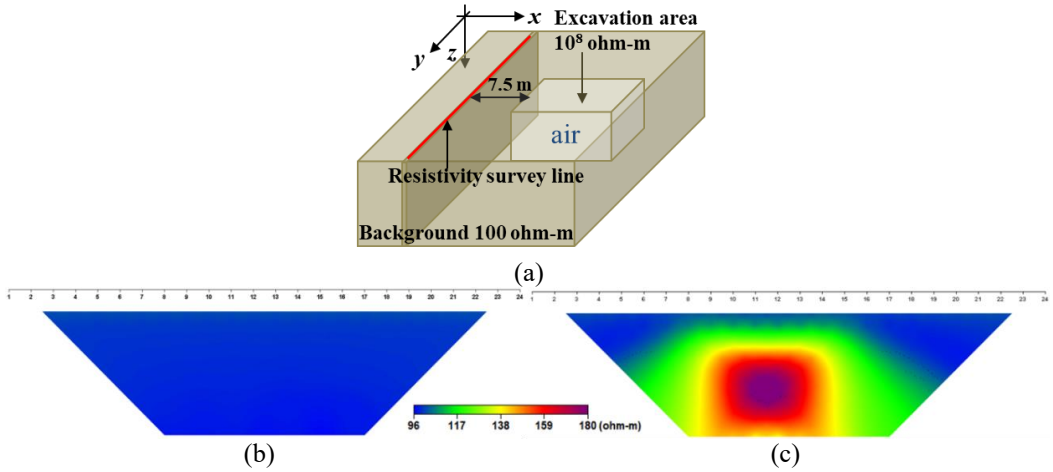

Fig. 7 (a) The 3D numerical model of homogeneous resistivity (100 ohm-m) including the excavation site, which had an air resistivity of 10^8 ohm-m. The survey line is the solid red line, which was 7.5 m from the excavation site. The configurations are the same as in the field survey described in Fig. 1(b). Apparent resistivity data from the homogeneous models (b) without the excavation site and (c) with the excavation site

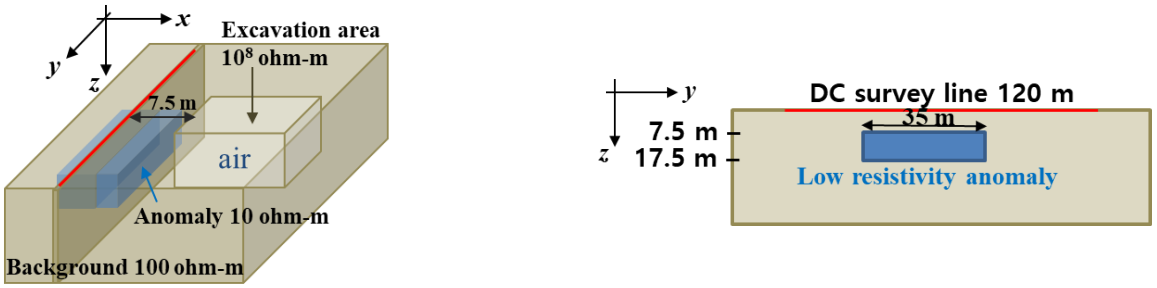

Fig. 8 (a) The loosened zone with a resistivity of 10 ohm-m was added to the model from Fig.7(a). (b) Cross-sectional view of the *yz* axis below the survey line (solid red line)

respectively, and was located at a depth of 7.5–17.5 m (Fig. 8). The electrode spacing was the same as in the field survey. The apparent resistivity data of the 3D model including both the excavation site and loosened zone became resistive and was more distorted by the excavation site in comparison with the homogeneous model including the loosened ground anomaly (Fig. 9(b)). The distorted data were corrected to remove the effect of excavation by using the ratio of changes in resistivity caused by the excavation site, as calculated by Eq. (1). The corrected apparent resistivity data (Fig. 9(c)) were similar to the data obtained by 3D modeling including the loosened zone (Fig. 9(a)).

Using DC2dpro software (Kim 2009), 2D inversions were conducted with three iterations for the ERT data obtained from the homogeneous and excavation site 3D models with the loosened ground anomaly (Figs. 9(a) and (b)) and corrected data (Fig. 9(c)). Inversion of the distorted data revealed a resistive anomaly below the conductive anomaly (Fig. 9(e)), while the corrected data clearly showed a conductive anomaly in the homogeneous background (Fig. 9(f)). In the conductive anomaly region, the average resistivity values for the corresponding inverse blocks were 42.6 and 33.38 ohm-m before and after considering the effects of the excavation site, respectively. The resistivity of the conductive loosened zone was set to 10 ohm-m, and inversion considering the excavation produced much more accurate results.

The 3D modeling and 2D inversion were repeated for a two-layered earth model with the same conductive loosened zone and excavation site. The resistivity of the first layer was set to 100 ohm-m based on the apparent resistivity near the surface at this site. The second layer of 1,000 ohm-m was set to start at a depth of 23.3 m based on the actual bedrock depth. The 2D inversion results (Figs. 9(g)-9(i)) showed that the effect of the high-resistivity excavation site was stronger in the resistive bedrock and the conductive loosened zone was also identified more precisely by removing the effect of excavation. Therefore, 2D inversion should be performed with consideration of the effects of excavation sites.

5. Inversion of ERT data obtained at the study site

We conducted 2D and 3D inversions for the field data obtained from the subsidence area. In the 2D inversion, the excavation effect was considered through the data correction method. The 3D inversion was performed using a

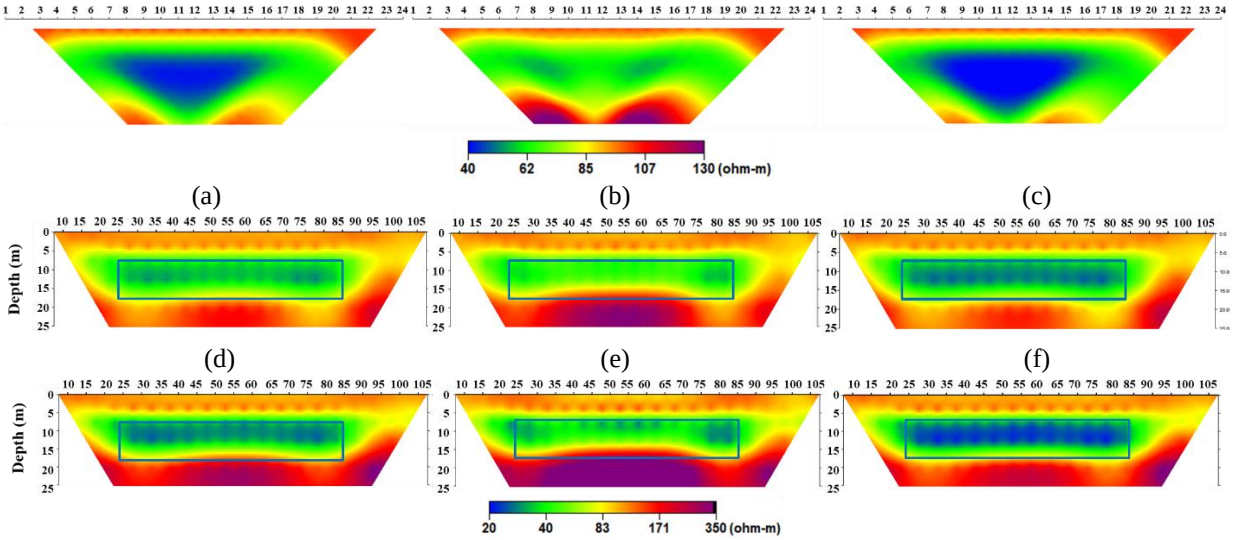

Fig. 9 Pseudo sections of apparent resistivity simulated by the numerical models shown in Fig. 8, which have a conductive loosened zone (a) without and (b) with an excavation site. The apparent resistivities (b) were corrected by removing the effect of excavation (c). The 2D inversions performed for (a)-(c) are shown in (d)-(f), respectively. The 2D inversion results ((g)-(i)) for data obtained using two-layered earth models. The results of (g)-(i) are similar with (d)-(f), except for the presence of a basement. The blue solid rectangles in each figure indicate the location of the conductive loosened zone

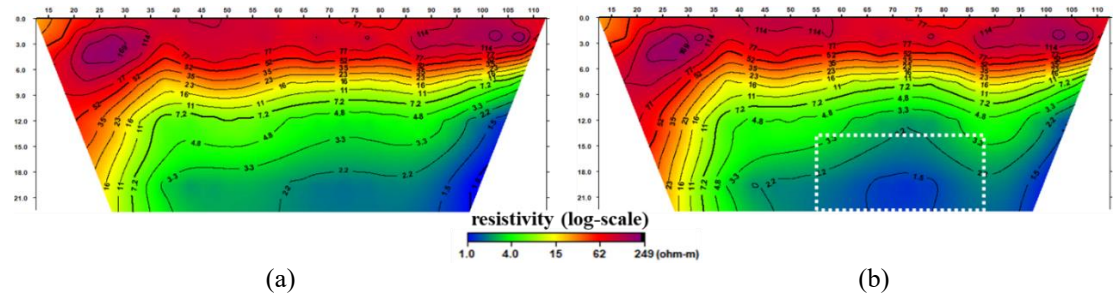

Fig. 10 Results of 2D inversion performed for field data (a) before and (b) after removing the effects of the excavation site

in-house 3D inversion algorithm that could consider the effects of excavation (Kim *et al*. 2022, Appendix A). In the 3D inversion, the high-resistivity excavation site was within the calculation area and influenced the modeling. It was excluded when the inversion was conducted, and the model was iteratively updated.

5.1 The 2D inversion with adjustment for the effects of excavation

The field data in the region where subsidence occurred was corrected for the 2D inversion using the ratio of resistivity change (Eq. (1)). The ratio was calculated through field-scale modeling of a homogeneous numerical excavation model considering the sizes of the actual excavation and survey line in the subsidence site. Field apparent resistivity data were corrected using the ratio in the same way as in the numerical test.

Inversion of the raw data using DC2dpro software revealed a conductive zone on the right boundary of the survey line (Fig. 10(a)). In contrast, inversion of corrected data revealed a conductive anomaly located from 55 m to about 90 m of the survey line, which leaded to the boundary of the survey line. The anomaly can be interpreted as a loosened zone and appeared in the area adjacent to the excavation site (Fig. 10(b)). The surface settlement measured at G3-6 appeared to be relatively large. The location of G3-4 was near the center of the survey line and adjacent to the excavation site, while G5 and G6 were located on the right side of the survey line at the boundary of the excavation site. After considering the surface settlement in the 2D inversion, the underground loosened zone was deemed likely to extend from the center to the right boundary of the survey line. Correction of distorted data through consideration of the excavation site aided localization of the loosened zone.

5.2 The 3D inversion including the excavation site

Using the algorithm developed by Kim *et al.* (2022), 3D inversion of the field ERT data considering the effects of the excavation site was performed. For the 3D inversion, an

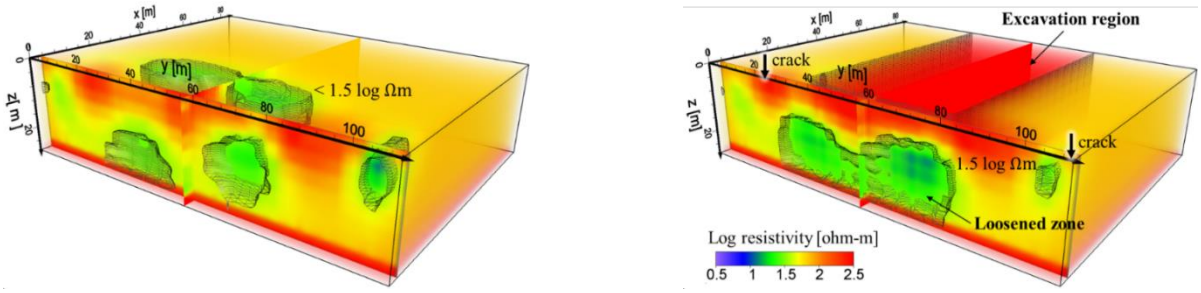

(a) (b)

Fig. 11 The 3D inversion results of the field ERT data shown in Fig. 6 without considering the excavation site (a) and considering the excavation site (b). The recovered cross section below the survey line is shown for the yz-plane and reveals a loosened zone < 1.5 log Ωm. The black solid arrows are the locations of surface cracks

initial model with an excavation site was composed of two layers of alluvial material and bedrock, whose resistivities were the average value of the measured apparent resistivities and 1000 ohm-m, respectively. The excavation region, whose resistivity was 10^8 ohm-m, was excluded from the inversion blocks, while it was included in the forward model simulation done using the 3D algorithm (Kim *et al.* 2022). For comparison, 3D inversion not considering the excavation site was also conducted.

The inversion result without considering the excavation site had conductive anomalies under the survey line as well as in the excavation site (Fig. 11(a)). The conductive anomaly in the excavation site was wrong anomaly. In contrast, the 3D inversion considering the excavation site showed conductive anomaly mainly in the deep area in the middle of the survey line (Fig. 11(b)). The conductive anomaly at a depth of 8 m was interpreted as a loosened zone because large subsidence occurred near the center of the survey line in that area. Considering that the settlements to the southwest of the area in which the second subsidence event occurred, analyzed by inclinometers G1−6, were relatively large, the more conductive area well-matched the area with greater subsidence.

6. Conclusions

Electrical resistivity tomography was conducted along a survey line in an urban area where ground subsidence occurred due to ground excavation. Changes in the GL were monitored during the excavation, and indicated that subsidence occurred after rapid outflow of groundwater and soil. Before interpreting the ERT data, the effects of the excavation site were analyzed to determine how it affects data and inversion results. A 2D inversion of the corrected field ERT data correctly identified the major loosened zone in the ground subsidence area. Further 3D inversion of the distorted data with consideration of the excavation site was performed to locate the loosened zone with higher accuracy.

A 2D inversion with consideration of the excavation site had the limitation of being less reliable than a 3D inversion, but also had the advantage of being able to quickly identify the loosened zone without distortion of the excavation site. Thus, ERT along a survey line could be effective for monitoring loosened zones during excavation work.

Acknowledgments

The research described in this paper was financially supported by Korea Spent Nuclear Fuel (iKSNF) and Korea Foundation of Nuclear Safety (KOFONS) grant funded by the Korea government (Nuclear Safety and Security Commission, NSSC) (No. 2109092-0121-WT112) and Korea Environment Industry & Technology Institute (KEITI) through Subsurface Environmental Managements (SEM) Projects, funded by Korea Ministry of Environment (MOE) (NO. RS-2023-00230833).

References

Arango-Galván, C., Torre-González, B.D.L., Chávez-Segura, R.E., Tejero-Andrade, A., Cifuentes-Nava, G. and Hernández-Quintero, E. (2011), "Structural pattern of subsidence in an urban area of the southeastern Mexico Basin inferred from electrical resistivity tomography", *Geofís. Int.*, **50**(4), 401-409. https://doi.org/10.22201/igeof.00167169p.2011.50.4.152.

Cardarelli, E., Di Filippo, G. and Tuccinardi, E. (2006), "Electrical resistivity tomography to detect buried cavities in Rome: a case study", *Near Surf. Geophys.*, **4**(6), 387-392. https://doi.org/10.3997/1873-0604.2006012.

Cárdenas-Soto, M., Escobedo-Zenil, D., Tejero-Andrade, A., Nava-Flores, M., Vidal-García, M.C. and Natarajan, T. (2020), "Exploring a near-surface subsidence over a rehabilitated underground mine through ambient seismic noise tomography in combination with other geophysical methods", *Near Surf. Geophys.*, **18**(5), 483-495. https://doi.org/10.1002/nsg.12108.

Chávez, R.E., Cifuentes-Nava, G., Hernández-Quintero, J.E., Vargas, D. and Tejero, A. (2014), "Special 3D electric resistivity tomography (ERT) array applied to detect buried fractures on urban areas: San Antonio Tecómitl, Milpa Alta", *México. Geofis. Int.*, **53**(4), 425-434. https://doi.org/10.1016/S0016-7169(14)70076-5.

Constable, S.C., Parker, R.L. and Constable, C.G. (1987), "Occam's inversion: A practical algorithm for generating smooth models from electromagnetic sounding data", *Geophysics*, **52**(3), 289-300. https://doi.org/10.1190/1.1442303.

De Giorgi, L. and Leucci, G. (2014), "Detection of hazardous cavities below a road using combined geophysical methods", *Surv. Geophys.*, **35**(4), 1003-1021. https://doi.org/10.1007/s10712-013-9277-4.

Fountain, L.S. (1975), "Evaluation of high-resolution earth resistivity measurement techniques for detecting subsurface cavities in a granite environment", *Nat. Tech. Information*

Service, U. S. A. https://doi.org/10.21236/ada018281.
Genis, M., Akcin, H., Aydan, O. and Bacak, G. (2018), "Investigation of possible causes of sinkhole incident at the Zonguldak Coal Basin, Turkey", *Geomech. Eng*., **16**(2), 177-185. https://doi.org/10.12989/gae.2018.16.2.177.
Han, N., Nam, M.J., Kim, H.J., Lee, T.J., Song, Y. and Suh, J.H. (2008), "Efficient three-dimensional inversion of magnetotelluric data using approximate sensitivities", *Geophys. J. Int*., **175**(2), 477-485. https://doi.org/10.1111/j.1365-246X.2008.03894.x.
Hong, J., Ji, Y., Oh, S. and Choi, S. (2015), "A geophysical survey of subsidence area around limestone mine sites", *Geophys. Geophys. Explor*., **18**(4), 207-215. https://doi.org/10.7582/gge.2015.18.4.207.
Jang, H., Song, S.Y., Kim, B. and Nam, M.J. (2018), "Strategy for improving the resolution of electrical-resistivity inversions for detecting soft ground at shallow depths (~ 10 m)", *J. Eng. Geol*., **28**(3), 367-377. https://doi.org/10.9720/kseg.2018.3.367.
Karaoulis, M.C., Kim, J.H. and Tsourlos, P.I. (2011), "4D active time constrained resistivity inversion", *J. Appl. Geophys*., **73**(1), 25-34. https://doi.org/10.1016/j.jappgeo.2010.11.002.
Kersten, T., Kobe, M., Gabriel, G., Timmen, L., Schön, S. and Vogel, D. (2017), "Geodetic monitoring of subrosion-induced subsidence processes in urban areas", *J. Appl. Geod*., **11**(1), 21-29. https://doi.org/10.1515/jag-2016-0029.
Kidanu, S., Varnavina, A., Anderson, N. and Torgashov, E. (2020), "Pseudo-3D electrical resistivity tomography imaging of subsurface structure of a sinkhole—A case study in Greene County, Missouri", *AIMS. Geosci*., **6**(1), 54-70. https://doi.org/10.3934/geosci.2020005.
Kim, B., Joung, I., Cho, A., Shin, D.K., Han, Y. and Nam, M.J. (2022), "Monitoring the perturbation zone near a foundation excavation with electrical resistivity tomography: Comparison between time-lapse 3D and 2D inversions in single-profile study", *J. Appl. Geophys*., 104-772. https://doi.org/10.1016/j.jappgeo.2022.104772.
Kim, J.H., Yi, M.J., Hwang, S.H., Song, Y., Cho, S.J. and Synn, J.H. (2007), "Integrated geophysical surveys for the safety evaluation of a ground subsidence zone in a small city", *J. Geophys. Eng*., **4**(3), 332-347. https://doi.org/10.1088/1742-2132/4/3/s12.
Kong, S.M., Kim, D.M., Lee, D.Y., Jung, H.S. and Lee, Y.J. (2018), "Field and laboratory assessment of ground subsidence induced by underground cavity under the sewer pipe", *Geomech. Eng*., **16**(3), 285-293. https://doi.org/10.12989/gae.2018.16.3.285.
Lee, K.H., Park, J.H., Park, J., Lee, I.M. and Lee, S.W. (2019), "Electrical resistivity tomography survey for prediction of anomaly inmechanized tunneling", *Geomech. Eng*., **19**(1), 93-104. https://doi.org/10.12989/gae.2019.19.1.093.
Leucci, G. and De Giorgi, L. (2014), "Cetotheridae, Mysticete Whale, fragment of mandibular detection using GPR method", *Proceedings of the 15th International Conference on Ground Penetrating Radar*, IEEE, 108-112. https://doi.org/10.1109/icgpr.2014.6970395.
Liu, N., Huang, Q.B., Fan, W., Ma, Y.J. and Peng, J.B. (2018), "Seismic responses of a metro tunnel in a ground fissure site", *Geomech. Eng*., **15**(2), 775-781. https://doi.org/10.12989/gae.2018.15.2.775.
Liu, R., Sun, H., Qin, J. and Zheng, Z. (2023), "A multi-geophysical approach to assess potential sinkholes in an urban area", *Eng. Geol*., 107-100. https://doi.org/10.1016/j.enggeo.2023.107100.
Samouëlian, A., Cousin, I., Tabbagh, A., Bruand, A. and Richard, G. (2005), "Electrical resistivity survey in soil science: a review", *Soil Tillage Res*., **83**(2), 173-193. https://doi.org/10.1016/j.still.2004.10.004.
Sharma, S. and Verma, G.K. (2015), "Inversion of electrical resistivity data: a review", *Int. J. Comput. Syst. Eng*., **9**(4), 400-406. https://doi.org/10.5281/zenodo.1106169.
Smith, D.L. (1986), "Application of the pole-dipole resistivity technique to the detection of solution cavities beneath highways", *Geophys*., **51**(3), 833-837. https://doi.org/10.1190/1.1442135.
Tsourlos, P.I., Szymanski, J.E. and Tsokas, G.N. (1999). The effect of terrain topography on commonly used resistivity arrays. Geophysics, 64(5), 1357-1363. https://doi.org/10.1190/1.1444640.
Ungureanu, C., Priceputu, A., Bugea, A.L. and Chirică, A. (2017), "Use of electric resistivity tomography (ERT) for detecting underground voids on highly anthropized urban construction sites", *Procedia. Eng*., **209**, 202-209. https://doi.org/10.1016/j.proeng.2017.11.148.
Prudhomme, K.D., Khalil, M.A., Shaw, G.D., Speece, M.A., Zodrow, K.R. and Malloy, T.M. (2019), "Integrated geophysical methods to characterize urban subsidence in Butte, Montana, USA", *J. Appl. Geophys*., **164**, 87-105. https://doi.org/10.1016/j.jappgeo.2019.03.004.
Ramirez, R.A., Lee, G.J., Choi, S.K., Kwon, T.H., Kim, Y.C., Ryu, H.H. and Hyun, C. (2022), "Monitoring of construction-induced urban ground deformations using Sentinel-1 PS-InSAR: The case study of tunneling in Dangjin", *Korea. Int. J. Appl. Earth Obs. Geoinf*., **108**, 102721. https://doi.org/10.1016/j.jag.2022.102721.
Vickery, A.C. and Hobbs, B.A. (2002). "The effect of subsurface pipes on apparent-resistivity measurements", *Geophys. Prospect*., **50**(1), 1-13. https://doi.org/10.1046/j.1365-2478.2002.00295.x.
Yun, H.S., Lee, J.Y., Yang, D.Y. and Hong, S.S. (2007), "Areal distribution ratio of rock ffes with geologic ages in the Gyeonggi-Seoul-Incheon Areas", *J. Petrol. Soc. Korea*, **16**(4), 208-216. https://koreascience.kr/article/JAKO200718259610682.page.

IC

Appendix A

- 3D inversion algorithm considering the excavation site

The 3D DC inversion was performed by iteratively solving the following nonlinear problem

$$\Delta\mathbf{d} = \mathbf{j}\Delta\mathbf{m} \tag{A1}$$

where $\Delta\mathbf{d}$ is the vector of the difference between the observed and numerically simulated data, $\Delta\mathbf{m}$ **is** a model correction vector, and $\mathbf{j}$ is a sensitivity matrix. Solutions of (Eq. (A1)) that yield $\Delta\mathbf{m}$ values are numerically unstable; therefore, constraints are required. Model roughness is often minimized using an objective function Φ (Han *et al*. 2008)

$$\Phi(\mathbf{m}^k) = \left\|\Delta\mathbf{d}^k - \mathbf{j}^k\Delta\mathbf{m}^k\right\|^2 + \lambda^2\left[\left\|\mathbf{cm}^k\right\|\right]^2 \tag{A2}$$

where $\mathbf{c}$ is a second-order difference operator quantifying model roughness, $\mathbf{m}^k$ is the model at the k-th iteration, and λ is the Lagrange multiplier. λ balances the model misfit ($\|\Delta\mathbf{d}^k - \mathbf{j}^k\Delta\mathbf{m}^k\|$) with the spatial constraints ($\|\mathbf{cm}^k\|$). Smoothing constraint is widely used in spatial domain models using least-squares inversion. Smoothness constraint forces spatial model parameters to change gradually by minimizing the primary or secondary differentiations (Constable *et al*. 1987). Minimizing the objective function in (Eq. (A2)) is equivalent to solving the following observational equation

$$\begin{bmatrix}\mathbf{j}^k \\ \lambda\mathbf{c}^k\end{bmatrix}\Delta\mathbf{m}^k = \begin{bmatrix}\Delta\mathbf{d}^k \\ -\lambda\mathbf{cm}^k\end{bmatrix} \tag{A3}$$

A modified Gram–Schmidt method is used to solve (Eq. (A3)) (Han *et al.* 2008), which yields $\Delta\mathbf{m}$; this is then added to $\mathbf{m}$ when the model is updated. This procedure is repeated until the misfit between the measured and modeled data decreases to an acceptable level.

When inverting ERT data obtained near the excavation, we excluded the excavation site itself but included it when modeling the ERT signals. The excavation position and dimensions were known and could therefore be excluded from the inversion. When modeling the ERT signals in the presence of an air-filled excavation site (which distorts ERT responses), the excavation site is assumed to be a highly resistive body because the half-space condition deals with geometry only. The surface of the earth is usually considered to be a half-space. The resistive body of the excavation had the same resistivity as air, i.e., 10^8 ohm-m. Given the exclusion of the excavation site from the inversion, there was no need to add smoothing constraints to (Eq. (A2) or (A3)) when considering the inversion blocks between the excavation site and inversion domain during computation of the roughness matrix.